Design and Validation of a Haptic Ankle Platform for Physical Human-Machine Interaction

Matteo Cecamore[1], Igor Gaponov[2], Stuart C. Miller[3] and Ildar Farkhatdinov[4,5]

***Abstract*— The paper presents a new modular robotic ankle interface for physical human-robot physical interaction research. We describe the interface's mechanical design, control system, and its experimental validation. The experiments include the controller performance evaluation and haptic interaction trials with a human participant. The advantages of the presented interface include a modular design approach, portability, single-degree-of-freedom actuation, and adjustable ergonomic design. An impedance controller with an update rate of 10 kHz was implemented on a PC communicating with the motor controller using the CAN bus. Three tests were conducted to determine the system's performance. The first test measured the torque transmission capabilities of the platform, validating a gear-up transmission ratio of 20:1 from the theoretical design. The second test identifies the mechanical transfer function of the foot platform showing a cutoff frequency of 0.32 Hz. The third test checked the muscular activation of the Gastrocnemius Medialis and Tibialis Anterior muscles when walking on a virtual floor implemented on the platform. The peak muscular activation was compared to the output torque and angle of the system. Results showed a linear relationship between muscular activation and torque when in contact with the virtual floor. Future work includes controlling virtual jumping using a platform for each foot.**

I. INTRODUCTION

Robotic systems are efficient tools to provide active physical interaction capabilities in various human-machine interaction applications, for example, navigation in virtual reality (VR). In this paper, we present our progress on the design of an ankle interface that we aim to use for locomotion-based interaction in virtual reality.

Robotic ankle interfaces have been explored widely for applications that require physical human robot interactions [1]–[3]. However, no simple and portable solution exists for realistically simulating complex interactions such as walking, jumping, or climbing up slopes while providing sensory feedback to the user in virtual reality-based applications. The major challenge is the availability and suitability of the space in which the user is interacting with the VR interface. Walk-In-Place (WIP) interfaces for VR can be compact [4], portable, and more accessible. Current research includes various approaches such as gesture control systems [5], wearable sensors that measure joint motion [6], or platforms that can extract forces exerted by the users [7]. Current researched WIP platforms are still not fully accessible to impaired users since most require the user to be standing [8]. Seated foot platforms also have the benefit of allowing disabled users to interact with the environment without needing their full strength to walk or stand [9], [10]. However, research on seated foot platforms is mostly focused on ankle rehabilitation without trying to create a multipurpose design that could be used for applications such as human-machine interfaces for VR. To address this, a seated walk-in-place platform was developed recently [11]–[13], consisting of a one-degree-of-freedom ankle platform capable of converting foot tapping to a realistic gait in VR. But the system was used for both feet and was not capable of emulating more complex behaviours such as jumping.

Simulating exteroception on practical WIP platforms is still a challenge. A walk-in-place platform with an external tether could simulate walking on slopes [7], however, this is only effectively operated by a fully-abled person. More minimalist approaches successfully prove the use of specially

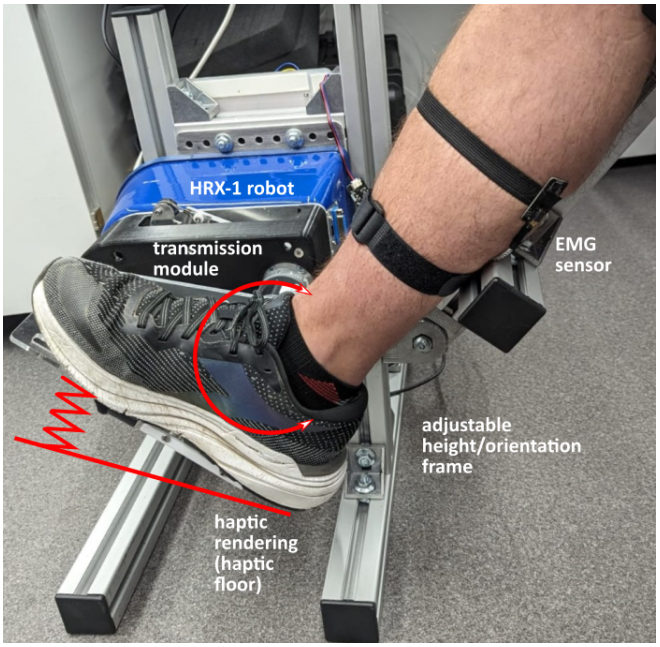

Fig. 1. Fully assembled foot platform being used with the left leg. The platform is mounted above the ground on aluminium rails. The mounting height can be easily adjusted. Optionally, the leg can be strapped on the same frame for more controlled movements.

*This work was supported by the UKRI EPSRC grant EP/T027746/1 and EPSRC PhD DTP studentship to Matteo Cecamore.

[1]School of Electronic Engineering and Computer Science, Queen Mary University of London, UK. m.cecamore@qmul.ac.uk

[2]Department of Computer Science, University College London, UK.

[3]William Harvey Research Institute, Barts & The London School of Medicine & Dentistry. Queen Mary University of London, UK

[4]School of Biomedical Engineering and Imaging Sciences, King's College London, London, UK, i.farkhatdinov@qmul.ac.uk

[5]School of Engineering and Materials Science, Queen Mary University of London, UK

angled shoes to create the illusion of sloped movement [14]. However, this is not a general approach and it cannot adapt to a changing virtual environment.

The effectiveness of current VR walking solutions has mostly been evaluated using metrics targeting locomotion performance and usability, but biometrics such as ECG and EMG have been less explored [15]. Conversely, haptic platforms for clinical applications present extensive use of biometrics to evaluate the rehabilitative potential of the design [16]–[18]. Additionally, some have used EMG data to predict user motion to more effectively assist or impede walking [19]. Thus, the user's muscular activation (EMG), heart rate, and oxygen consumption can be used to compare the user's experience between simulated and real environments [7], or to create a dynamically adaptive interface for users with specific muscular weaknesses [16], [20].

A new one degree of freedom of walk-in-place foot platform with haptic feedback is proposed (see Fig. 1). The goal of this interface is to investigate how a one degree of freedom, seated, haptic foot platform can be used to effectively control different types of jumping in virtual reality. It is a compact, modular, and easily adjustable design which will allow for more efficient experimental setups. A simulated virtual floor impedance controller has also been implemented to test the effectiveness of the design in eliciting muscular activation in the user.

II. ANKLE INTERFACE DESIGN

A. General Description

Our ankle robotic system for physical human-robot interaction research is based on the customised extension of the commercial HRX-1 robot (Human Robotix Ltd, London, UK[1]). The HRX-1 is a single degree of freedom robot with a DC actuator (EC Maxon motor), torque and angular position sensors, and an electronic controller for interfacing with the dedicated computer software. HRX-1's actuator can produce programmable torques of required magnitudes and directions that can be applied to a user's joints (e.g. wrist, elbow, ankle). We designed a cable-driven transmission module that was attached to the HRX-1 robot to increase the output torque capacity and facilitate integration with an ankle platform. A user's foot is attached to the interface through a custom design ergonomic footplate connected to the output shaft of the transmission module. The user's shank is attached to the adjustable base support frame of the robot to align the ankle's center of rotation with the center of rotation of the foot platform and the transmission module's output shaft.

B. Mechanical Design

A cable-based pulley system was chosen as the transmission type for the ankle add-on module for the HRX-1 robotic platform as shown in Fig. 1. A direct drive design was chosen for its low friction and mechanical backdrivability, allowing for bidirectional haptic transparency. The platform has a single degree of freedom and it allows for

[1]https://www.humanrobotix.co.uk

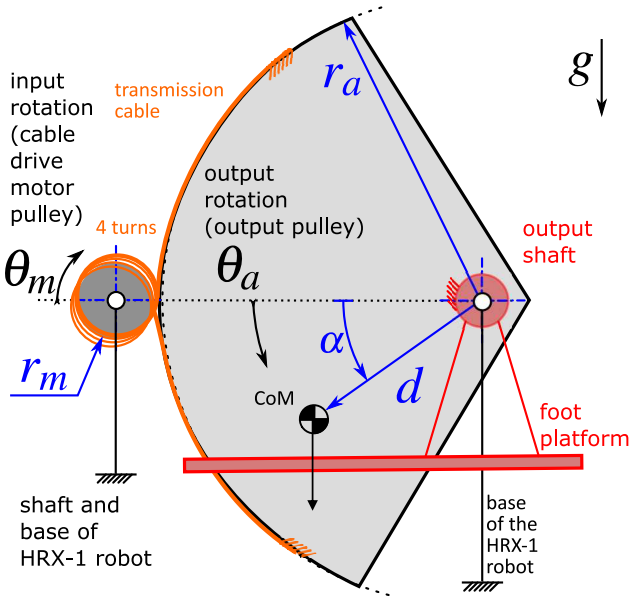

Fig. 2. Schematic representation of the cable drive kinematics used for the ankle platform. The HRX-1 motor is connected to the larger pulley through a single transmission cable. The larger pulley is connected to the output shaft, which connects to the foot attachment (not pictured). The center of mass calculation includes the mass of the foot platform attachment.

TABLE I
TABLE OF MECHANICAL VALUES

Name	Value	Unit	Description
α	43	degree	angle of CoM from x_{shaft}
θ_a	[-41.5 +41.5]	degree	angle of the output shaft
θ_m		degree	motor angle
m	0.99	kg	platform's mass
J_a	$9.44{\cdot}10^{-3}$	$kg \cdot m^2$	inertia about the shaft axis
d	5.1	cm	distance of CoM from shaft
r_m	1.5	cm	motor pulley radius
r_a	15	cm	output pulley radius
n	-20		transmission ratio

foot dorsi/plantarflexion. The haptic floor is rendered by a motor acting on a transmission module connected to a plate on which the foot rests. The free body diagram in Fig. 2 shows the main control variables and the platform's initial configuration. Table I shows the mechanical variables and constants required to control the robot. The values for the Center of Mass are calculated from CAD software. As shown in Fig. 3, the maximum range of motion of the output foot plate is 83°, and its maximum and minimum positions can be manually shifted by 30° by remounting the hub on the output shaft. A Maxon EC90 Brushless DC Motor (600 W, 2 Nm peak torque) was connected to the small pulley, with a torque output of 40 Nm. A steel cable (Tecni 0.75 mm nylon coated, 7x19 core stainless steel 316) is wound around the motor pulley four times and tensioned.

C. Electrical Design

The electrical setup as shown in Fig. 4 contains a CAN bus for digital communication, the personal computer (PC),

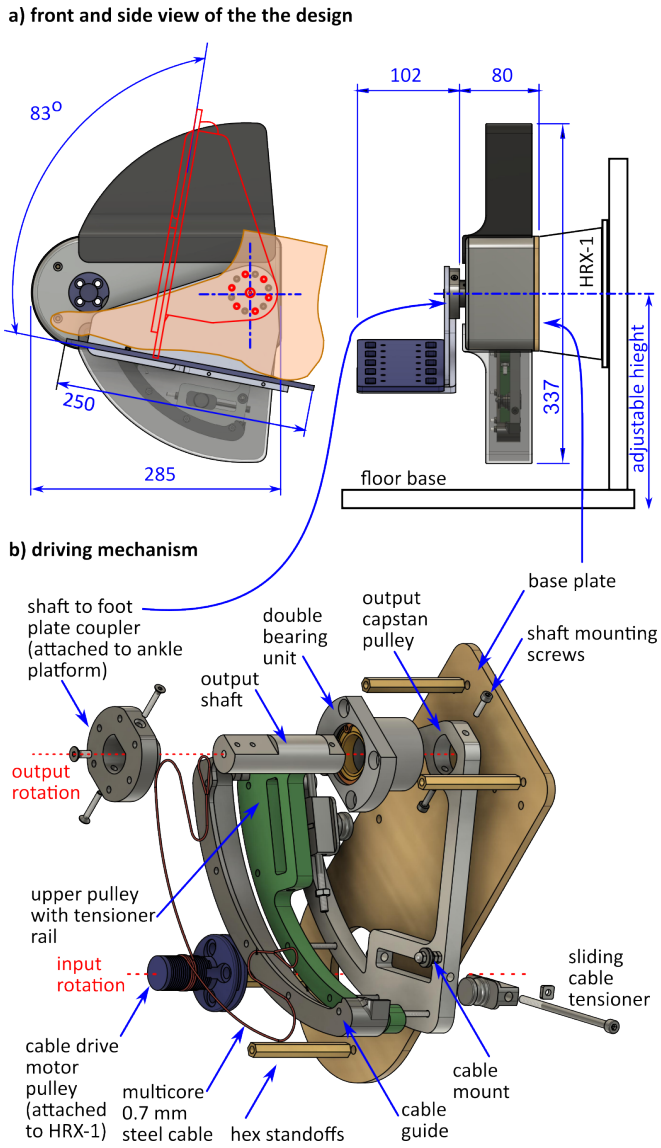

Fig. 3. **a)** Foot Platform Views and Dimensions in millimeters. The figure shows the maximum range of motion of the platform to accommodate a user who is sitting with a leg at a 45◦ angle from the floor. The platform has a maximum positive angle of 8◦ and a negative angle of 75◦ from the floor. At higher angles, the platform hits hard stops. **b)** Exploded view of the pulley transmission. A single cable is mounted and tensioned on the larger pulley on both sides. The cable turns 4 times around the smaller pulley to ensure enough friction. The large pulley is made of aluminium, with the outer face protected by a thin 3D printed layer.

Maxon EPOS 4 motor driver, and TI Launchpad F28069 microcontroller board. The PCAN to USB device and PCAN-View from PEAK systems is a high-frequency CAN interface and logger. DFRobot Oymotion surface EMG sensors are used to measure muscular activation. The TI board converts the analog EMG signal into CAN messages at a rate of 2.5 kHz. The Maxon motor driver uses the CANOpen protocol for bidirectional communication of the motor position, velocity, and current inputs at a variable rate of up to 2.5 kHz. The PC runs the control software at a fixed update frequency of 10 kHz.

D. Control System

The impedance controller, shown in Fig. 5 was used to simulate a virtual floor with gravity compensation. The velocity from the motor encoder was calculated using the discrete-time derivative of the motor encoder position.

The torque required to cancel the effect of gravity was calculated geometrically using known constants. The only variable affecting the calculation is the output shaft's position θ_a as shown:

$$Z_g(\theta_a) = \frac{mgd\cos(\alpha - \theta_a)}{n} \tag{1}$$

The linearised differential equation for the plant P(s) is modeled as a spring-damper system with a gravity component, where B is the unknown friction of the system, J is the pulley's inertia and Z_g is the gravity compensation:

$$J_a\ddot{\theta}_a + B\dot{\theta}_a + Z_g(\theta_a) = \tau_{out} \tag{2}$$

The transmission ratio Z_t for θ_a from the from the motor encoder's position is:

$$Z_t = \frac{2\pi}{25600n}\theta_m. \tag{3}$$

The velocity signal from the encoder was filtered using a 5 Hz low pass filter to mitigate the effects of a low signal resolution.

$$G(s) = \frac{10\pi}{s + 10\pi}. \tag{4}$$

The virtual floor's impedance controller $C(s)$ can be modeled as a sum of torques calculated from the motor's position and velocities. This controller is only designed to compensate for the effect of gravity on the plant, while the other components simulate a virtual spring (k) - damper (b) system based on the user's interaction. The plant's inertia and friction were not compensated.

$$\tau_{in} = Z_g(\theta_a) + k\theta_a + b\dot{\theta}_a. \tag{5}$$

The complete negative feedback control system is defined as the following, where G(s) is the feedback transfer function as the low pass filter, including the encoder transmission Z_t, P(s) is the plant and C(s) is the impedance controller:

$$\frac{Y(s)}{X(s)} = \frac{C(s)P(s)}{1 - Z_t G(s)C(s)P(s)}. \tag{6}$$

III. EXPERIMENTAL VALIDATION

A. Torque Transmission Properties

To verify and characterize the mechanical properties of the platform, the transmission performance of the pulley system was tested. The foot attachment was disconnected and the platform's output shaft output was fixed to the base. Two torque sensors were mounted, one between the motor shaft and pulley, to measure the input torque, and one between the output shaft and the base frame, to measure the output torque. The TRT-100 torque transducers' signal was amplified using the ICA1H and calibrated using a linear voltage equation. A fixed current between -4 A to 4 A was sent to the motor

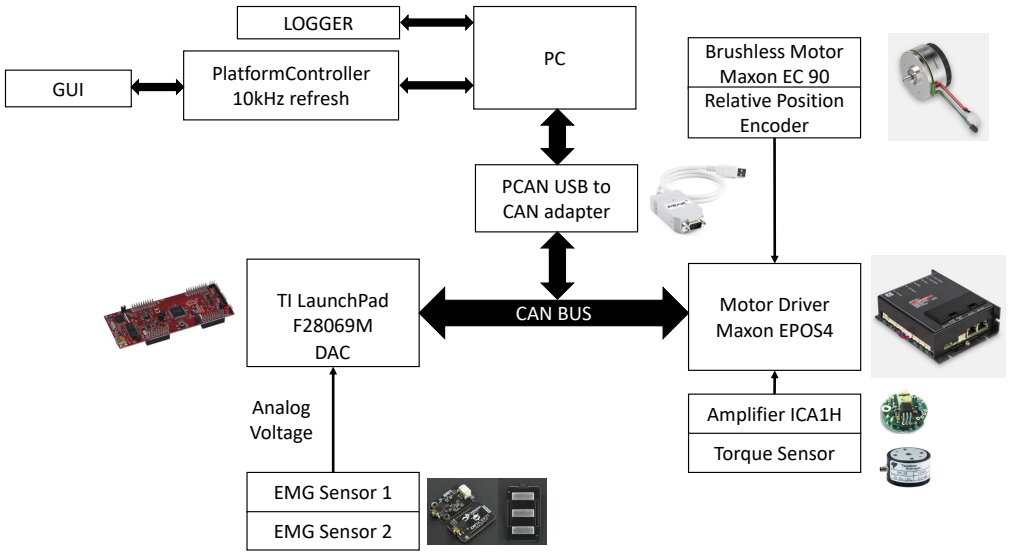

Fig. 4. Schematic of the electronic components used to control the platform. The Maxon EPOS4 motor driver controls the 600 Watt Brushless motor using a current control loop and hall effect encoders. A 6400 counts per revolution relative encoder is used to monitor the motor position and speed. The TI F28069 board was used to relay the EMG signals to the CAN bus. A PC is used to log the variables on the CAN bus and run the digital control loop.

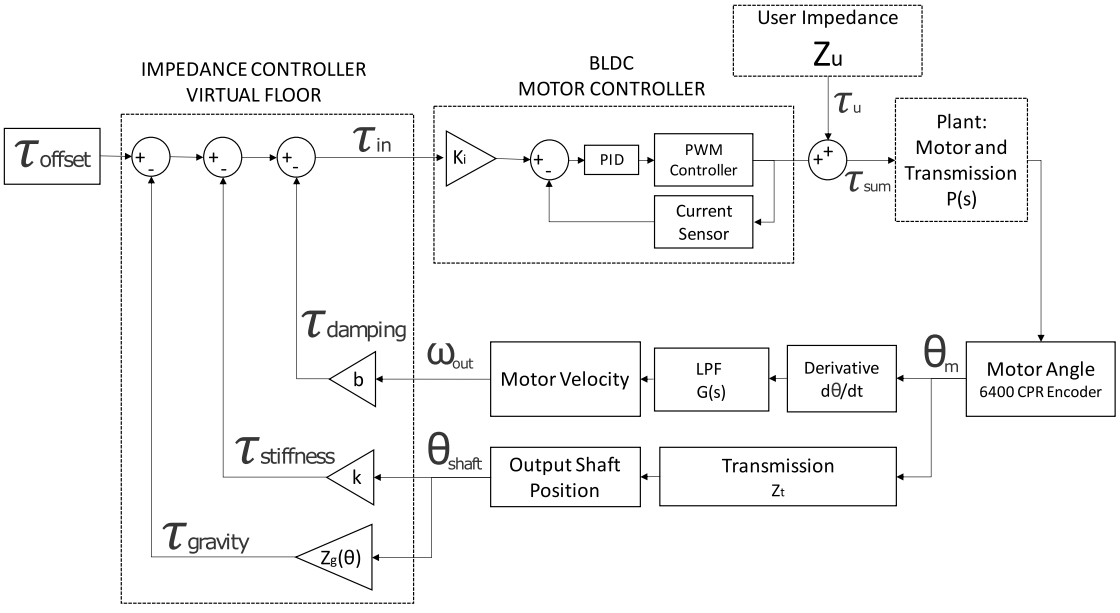

Fig. 5. Closed loop system with impedance and gravity controller for virtual floor simulation. The impedance controller sums the total amount of torque τ_{in} required to oppose the unknown user's input impedance Z_u. τ_{offset} is set to zero for this experiment. The EPOS4 motor controller has a built-in PID current sensing loop which is then multiplied by the motor's torque constant K_i to effectively control the required motor torque.

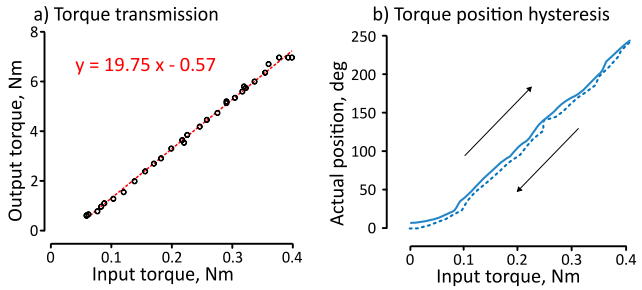

Fig. 6. **(a)** Graph showing the linear relationship between torque input torque and output torque. The best-fit line's slope is 19.95 indicating that the transmission ratio is near 20. The line's intercept is less than zero. **(b)** Relationship between the motor's input torque and the motor's final position after it has stopped moving. When the torque increases, the position increases linearly. Little hysteresis is observed starting from a 0 torque to 0.4 Nm (blue) and vice versa (dashed).

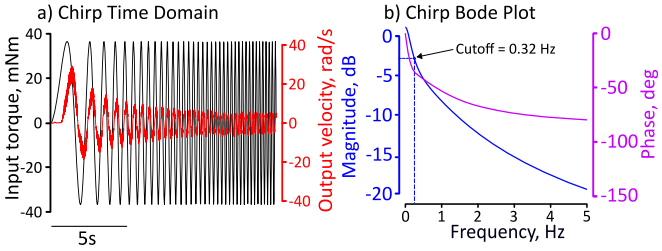

Fig. 7. **(a)** Time domain results of the frequency sweep of the torque input (blue) and the output velocity (orange). This is due to the high inertia and friction in the pulley system attached to the motor. **(b)** Results of the frequency analysis of the transfer function computed from the time domain data using the ratio between the motor velocity and the torque input.

drive, in 30 steps, corresponding to a maximum torque of 0.544 Nm. The results shown in Fig. 6(a), confirm that the transmission system is linear with a multiplier up to 19.75 times. The output position and torque relationship in Fig. 6(b) indicate that there is some elasticity in the system, most likely due to the flexibility of the transmission cable.

B. Mechanical System Identification

This test was designed to identify the plant's transfer function $P(s)$. The plant comprises the motor, the transmission assemblies, and the motor torque controller. The plant's dynamics were modeled as a spring, mass, and damper system, with a torque input and a velocity output. The robot was placed parallel to the floor to remove the effect of gravity and the output shaft was freely moving. An open loop chirp torque signal was sent to the motor driver and the motor's resulting speed was then recorded from its encoder. The output shaft's speed was not used for this since it was proven to be a fixed gain of about 1/20 from the motor. A chirp signal, with a linear frequency sweep between 0-5 Hz for 15 seconds, with 36 mNm of amplitude was applied. The second order transfer function was estimated using the 'tfest' function in MATLAB shown in (7):

$$P(s) = 100\frac{3.812s + 8.367}{s^2 + 7.671s + 6.539}. \tag{7}$$

The results, in Fig. 7, show that the system has a very low frequency response with a cutoff frequency of 0.32 Hz and a phase difference of up to -90°. This is useful to know when designing a virtual jump controller which may require higher impulse signals.

C. Virtual Floor Testing

The platform's effectiveness at generating a resistive virtual floor was tested by measuring the user's muscular activation using electromyography. A floor with a stiffness constant (k) of 7 Nm/rad and a damping constant (b) of 0.012 Nm/rad/s was inputted in the impedance controller. The haptic virtual floor was programmed to activate when the user's foot was at a 35° angle from the real floor, starting at a resting position of 45° from the floor. A single, fully abled male subject was instructed to sit in front of the platform and perform six repetitions, first by plantaflexing the foot until the end of their range of motion and then slowly dorsiflexing the foot until they are out of the virtual floor (see Fig. 1). This procedure was to test the concentric activation of the Gastrocnemius Medialis and the eccentric motion of the Tibialis Anterior. The activation was recorded using surface EMG electrodes. The electrodes were placed on the leg following the SENIAM guidelines. The torque input of the motor and the EMG activation were recorded. The signals were passed through a 50 Hz notch filter, a bandpass filter between 20 Hz and 400 Hz, then root mean squared and, finally a moving average filter with a window size of 2000 samples at a sampling frequency of 1000 Hz to derive the enveloped signal. The results, shown in Fig. 8(a), it can be seen that the Gastrocnemius Medialis activation reaches a peak when the motor's torque is maximum, while the peak activation of the Tibialis Anterior peaks when the torque is decreasing at a higher rate, clearly showing eccentric activation elicited by the virtual floor. Fig. 8(b) shows a clear relationship between platform torque and muscular activation, being more marked with the Gastrocnemius Medialis muscle. The dashed lines show a positively increasing linear fit for EMG vs torque measurements demonstrating that the platform is effective at eliciting a muscular response to a virtual floor by increasing its torque output.

IV. CONCLUSION

The proposed ankle interface demonstrated efficient control and haptic rendering capabilities. A cable-driven transmission efficiently transferred the HRX-1 robot torque to a user reaching potentially up to 40 Nm ankle torque which is sufficient for the majority of VR interaction tasks including haptic rendering of virtual walls (floors). Evaluation of the lower limb muscle activation demonstrated that our robot can be used as an interface that initiates a physiological response of the user's neuromuscular system. The identified cut-off frequency of the robot (approx. 0.3 Hz) can be evaluated as a limiting factor for the design of haptic interaction effects. We shall explore if the cut-off frequency can be increased by improving the quality of the control system using a torque controller and assembly by using stiffer cables and by reducing the inertia of the moving parts. The future aim is

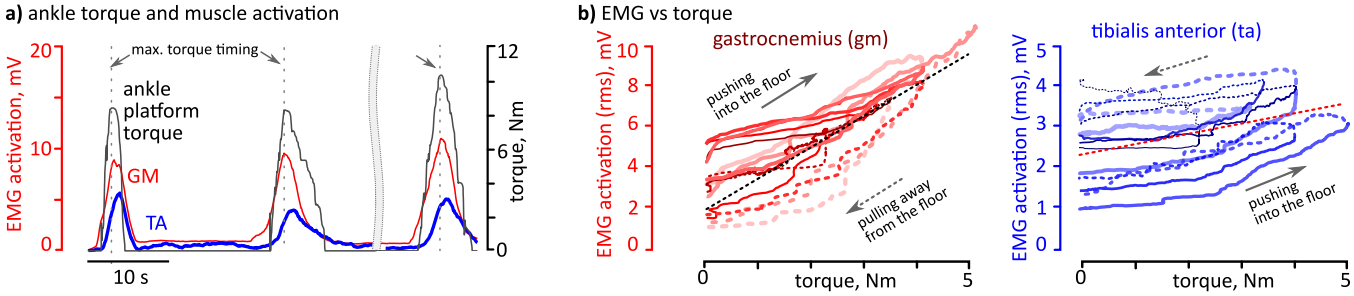

Fig. 8. Experimental results. **a)** Graph showing the relationship between effective motor torque and muscular activation measured using sEMG. As the motor's torque increases (grey), the Gastrocnemius activation reaches a peak (red). This represents the user pushing their foot on the virtual floor and the platform pushing against it, eliciting a concentric activation of the Gastrocnemius muscle. When the user starts releasing their foot in a controlled manner, this elicits an eccentric activation of the Tibialis Anterior (blue), which matches a decreasing motor torque. **b)** The graphs show the relationship between torque and activation across six repetitions on the virtual floor. The dashed lines show the average trend of the plots which is linear and positive, confirming that the platform is effective at eliciting a muscular response to a virtual floor.

to demonstrate that a single degree of freedom haptic ankle robotic device can be used to effectively control jumping movement in virtual reality. Therefore the future goal of this research is to design and evaluate a single degree of freedom haptic ankle interface for jumping in virtual reality.

References

[1] M. G. Alvarez-Perez, M. A. Garcia-Murillo, and J. J. Cervantes-Sánchez, "Robot-assisted ankle rehabilitation: A review," *Disability and Rehabilitation: Assistive Technology*, 2019.

[2] P. K. Jamwal, S. Hussain, and S. Q. Xie, "Review on design and control aspects of ankle rehabilitation robots," *Disability and Rehabilitation: Assistive Technology*, vol. 10, no. 2, pp. 93–101, 2015.

[3] Y. Huang, W. Lai, L. Cao, J. Liu, X. Li, E. Burdet, and S. J. Phee, "A three-limb teleoperated robotic system with foot control for flexible endoscopic surgery," *Annals of Biomedical Engineering*, vol. 49, pp. 2282–2296, 2021.

[4] C. Boletsis, "The new era of virtual reality locomotion: A systematic literature review of techniques and a proposed typology," *Multimodal Technologies and Interaction*, vol. 1, no. 4, 2017. [Online]. Available: https://www.mdpi.com/2414-4088/1/4/24

[5] Y. Hirao, T. Narumi, F. Argelaguet, and A. Lécuyer, "Revisiting walking-in-place by introducing step-height control, elastic input, and pseudo-haptic feedback," *IEEE Transactions on Visualization and Computer Graphics*, pp. 1–14, 2022.

[6] K. Junius, B. Brackx, V. Grosu, H. Cuypers, J. Geeroms, M. Moltedo, B. Vanderborght, and D. Lefeber, "Mechatronic design of a sit-to-stance exoskeleton," in *IEEE RAS & EMBS International Conference on Biomedical Robotics and Biomechatronics (BioRob)*, São Paulo, 2014.

[7] C. Parker, D. Carrier, and J. Hollerbach, "Validation of torso force feedback slope simulation through an energy cost comparison," in *First Joint Eurohaptics Conference and Symposium on Haptic Interfaces for Virtual Environment and Teleoperator Systems. World Haptics Conference*, 2005, pp. 446–451.

[8] N. C. Nilsson, S. Serafin, F. Steinicke, and R. Nordahl, "Natural walking in virtual reality: A review," *Comput. Entertain.*, vol. 16, no. 2, 4 2018. [Online]. Available: https://doi.org/10.1145/3180658

[9] M. Girone, G. Burdea, M. Bouzit, and V. Popescu, "A stewart platform-based system for ankle telerehabilitation," *Autonomous Robots*, vol. 10, pp. 203–212, 2001.

[10] M. Dong, W. Fan, J. Li, X. Zhu, X. Rong, Y. Kong, and Y. Zhou, "A new ankle robotic system enabling whole-stage compliance rehabilitation training," *IEEE/ASME Transactions on Mechatronics*, pp. 1490–1499, 2021.

[11] A. Otaran and I. Farkhatdinov, "Modeling and control of ankle actuation platform for human-robot interaction," in *Towards Autonomous Robotic Systems: 20th Annual Conference, TAROS 2019, London, UK, July 3–5, 2019, Proceedings, Part I 20*. Springer, 2019, pp. 338–348.

[12] ——, "A short description of an ankle-actuated seated vr locomotion interface," in *2021 IEEE Conference on Virtual Reality and 3D User Interfaces Abstracts and Workshops (VRW)*. IEEE, 2021, pp. 64–66.

[13] ——, "Haptic ankle platform for interactive walking in virtual reality," *IEEE Transactions on Visualization and Computer Graphics*, vol. 28, no. 12, pp. 3974–3985, 2022.

[14] Y. Zhang, J. Wu, and Q. Liu, "The sloped shoes: Influence human perception of the virtual slope," in *2022 IEEE Conference on Virtual Reality and 3D User Interfaces Abstracts and Workshops (VRW)*, 2022, pp. 826–827.

[15] E. S. Martinez, A. S. Wu, and R. P. McMahan, "Research trends in virtual reality locomotion techniques," in *2022 IEEE Conference on Virtual Reality and 3D User Interfaces (VR)*, 2022, pp. 270–280.

[16] K. Van Teeffelen, D. Dresscher, W. Van Dijk, and S. Stramigioli, "Intuitive impedance modulation in haptic control using electromyography," in *2018 7th IEEE International Conference on Biomedical Robotics and Biomechatronics (Biorob)*, 2018, pp. 1211–1217.

[17] I. Cikajlo, A. Krpič, and M. Gorišek-Humar, "Changes in emg latencies during balance therapy using enhanced virtual reality with haptic floor," in *2013 35th Annual International Conference of the IEEE Engineering in Medicine and Biology Society (EMBC)*, 2013, pp. 4129–4132.

[18] C. Casellato, A. Pedrocchi, G. Zorzi, L. Vernisse, G. Ferrigno, and N. Nardocci, "Emg-based visual-haptic biofeedback: A tool to improve motor control in children with primary dystonia," *IEEE Transactions on Neural Systems and Rehabilitation Engineering*, vol. 21, no. 3, pp. 474–480, 2013.

[19] D. Ao, R. Song, and J. Gao, "Movement performance of human robot cooperation control based on emg-driven hill-type and proportional models for an ankle power-assist exoskeleton robot," *IEEE Transactions on Neural Systems and Rehabilitation Engineering*, vol. 25, no. 8, pp. 1125–1134, 2017.

[20] J. M. Canino and K. B. Fite, "Haptic feedback in lower-limb prosthesis: Combined haptic feedback and emg control of a powered prosthesis," in *2016 IEEE EMBS International Student Conference (ISC)*, 2016, pp. 1–4.